Dynamics of femto- and nanosecond laser ablation plumes investigated using optical emission spectroscopy

B. Verhoff, S. S. Harilal, J. R. Freeman, P. K. Diwakar, and A. Hassanein
Center for Materials Under Extreme Environment and School of Nuclear Engineering, Purdue University, West Lafayette, Indiana 47907, USA

(Received 13 July 2012; accepted 9 October 2012; published online 2 November 2012)

We investigated the spatial and temporal evolution of temperature and electron density associated with femto- and nanosecond laser-produced plasmas (LPP) from brass under similar laser fluence conditions. For producing plasmas, brass targets were ablated in vacuum employing pulses either from a Ti:Sapphire ultrafast laser (40 fs, 800 nm) or from a Nd:YAG laser (6 ns, 1064 nm). Optical emission spectroscopy is used to infer the density and temperature of the plasmas. The electron density (n_e) was estimated using Stark broadened profiles of isolated lines while the excitation temperature (T_{exc}) was estimated using the Boltzmann plot method. At similar fluence levels, continuum and ion emission are dominant in ns LPP at early times (<50 ns) followed by atomic emission, while the fs LPP provided an atomic plume throughout its visible emission lifetime. Though both ns and fs laser-plasmas showed similar temperatures (~1 eV), the fs LPP is found to be significantly denser at shorter distances from the target surface as well as at early phases of its evolution compared to ns LPP. Moreover, the spatial extension of the plume emission in the visible region along the target normal is larger for fs LPP in comparison with ns LPP. © *2012 American Institute of Physics*. [http://dx.doi.org/10.1063/1.4764060]

I. INTRODUCTION

Laser ablation (LA) and laser-produced plasmas (LPP) have been studied extensively for more than 50 yr since the discovery of lasers in the 1960s. Plasma formation occurs when a high powered pulsed laser is focused onto a target such that the energy density surpasses the ablation threshold of the material. The laser-target interaction involves many processes, including heating, melting, vaporization, ejection of particles, and plasma creation and expansion.[1] The laser ablation craters and plasmas produced are dependent on laser beam parameters, such as pulse duration, energy, and wavelength; along with the target properties and surrounding conditions.

Many of the present applications of LPP have been developed in the past using nanosecond pulsed lasers by industry along with defense programs. The invention of chirped pulse amplification (CPA) techniques and the development of short pulse and reliable Ti-Sapphire lasers have led to new and improved applications of LPP technology. Prominent applications of LPP include surface smoothing,[2] micromachining,[3,4] laser surgery,[5] generation of collimated proton,[6] electron,[7] and neutron beams,[8] nanoparticle production,[9,10] ion beams[11] of various charge states, laser-ablation inductively coupled-plasma mass-spectrometry (LA-ICP-MS),[12] laser-induced breakdown spectroscopy (LIBS),[13] and pulsed laser deposition (PLD),[14] etc. Plasmas produced by ultrafast laser system have many benefits over typical ns lasers mainly due to the duration of the laser pulse (t_p) being shorter than the electron to ion energy transfer time (τ_{ei}) and heat conduction time (t_{heat}) ($\tau_{ei} \sim t_{heat} \gg t_p$). The heat affected zone (HAZ) of ns laser ablation is typically 100 μm to 1 mm, whereas a very small HAZ is noticed for fs laser ablation because of the limited penetration length of thermal diffusion.[15] With the shorter pulse duration of the femtosecond laser, the laser beam does not interact with the laser-induced plasma causing the laser energy to be fully deposited into the target; allowing for higher efficiency of material ablation.[16] An approximate representation of laser-target and laser-plasma coupling along with emission in the visible region is given in Figure 1 for ns and fs LA.[17,18] The benefits of the shorter pulse are that it provides higher precision during ablation and minimum HAZ to the target material compared to nanosecond lasers.[19] Femtosecond LA-ICP-MS generates uniform aerosol size distribution and in doing so it reduces elemental fractionation.[20] Also, ultrafast PLD minimizes the formation of droplets which are often seen with ns PLD.[21] Furthermore, fs LIBS is found to provide lower continuum compared to traditional ns LIBS.[22] As detailed in Figure 1, in the nanosecond LPP case, the leading edge of the laser interacts with the target surface creating plasma then the subsequent laser energy is imparted to the expanding plasma for further reheating causing a laser plasma interaction (LPI). It should be noted that the fs pulses have significantly lower laser ablation threshold fluence than the ns pulse and shorter pulses produce significantly more mass ablation at lower laser fluence levels.[23] Because of these key differences, recently many LPP applications have shifted from using ns pulses to shorter pulses in the fs range.

Plasma temperature and electron density are two important parameters that govern both kinetic and radiative properties of the plasma. Understanding the temperature and electron density of ns and fs LPP is very important for optimizing their parameters and conditions for various applications. These two parameters are required to develop and understand models for many plasma processes. There exists

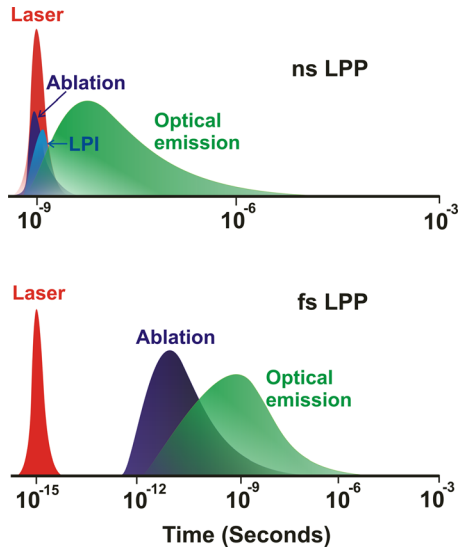

FIG. 1. Approximate time scales of nanosecond (top) and femtosecond (bottom) laser ablation and visible emission from the plasma.

several diagnostic tools for measuring the electron density which include Langmuir probe,[24] Thomson scattering,[25] microwave and laser interferometer,[26] and plasma spectroscopy.[27] Plasma density can also be determined using the Stark broadening method using specific spectral lines. Plasma spectroscopy is the simplest of these techniques and non-intrusive. The temperature of the plasma can be determined spectroscopically in many ways, including the shape of the continuum spectrum, the ratio of line intensity to the continuum, and from the ratio of integrated line intensities.

In this paper, we report on the spatio-temporal evolution of temperature and electron density of ns and fs laser ablated plasmas from brass targets generated in vacuum under similar laser fluence conditions. Though similar laser fluence conditions are used for the present studies, the power densities differ by more than five orders in magnitude. Line intensities of several Cu I were used to estimate the excitation temperature assuming that the plasma is in local thermodynamic equilibrium (LTE), while isolated Stark broadened Zn I lines were used for measuring density.

II. EXPERIMENTAL SETUP

The schematic of the experimental setup used in the present investigation is shown in Figure 2. Nd:YAG ns laser (Surelite I, Continuum lasers) provides 10 Hz, 6 ns full width half maximum (FWHM) pulses at a wavelength of 1064 nm. A combination of wave plate and polarizing cube were used for attenuating the energy of the ns pulse. The fs laser consists of mode-locked Ti-Sapphire oscillator (Synergy 20, Femtolasers) which generates ~35 fs pulses at 800 nm. The amplifier system (Pulsar, Amplitude Technologies) consists of stretcher, regenerative amplifier, multi-pass amplifier, and a compressor providing 10 Hz, 40 fs pulses. The pulse duration of the ns and fs lasers was measured using fast photodiodes (rise time ~300 ps) and a home-built autocorrelator, respectively. The energy of the fs laser output is varied using a half wave plate-polarizer combination positioned before the compressor gratings. For LPP generation, a brass target

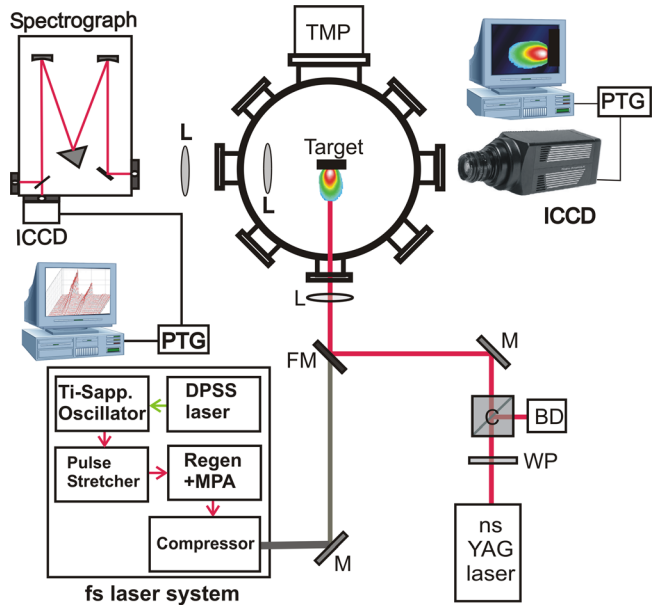

FIG. 2. Schematic of the experimental setup. The target is positioned in an evacuated chamber at $\sim 10^{-5}$ Torr. (TMP-turbomolecular pump, L-Lens, FM-flip mirror, M-mirror, BD-beam dump, WP-Wave plate, C-cube polarizer; ICCD-intensified charged couple device, PTG- pulse timing generator).

was positioned in an evacuated chamber with base pressure $\sim 10^{-5}$ Torr. The target is moved using an externally controlled xyz translator for providing a fresh surface. The p-polarized laser beam is focused onto the target using a plano convex lens along the target normal at an energy varying from 1 to 6 mJ. The estimated spot size area at the target surface was $\sim 1 \times 10^3\ \mu m^2$.

The plasma diagnostic instrumentation used include a 0.5 m focal length triple grating spectrograph (Acton, SP2500i) coupled with an intensified CCD camera (ICCD, Princeton Instruments PI-MAX) and timing generator. The two gratings used in the spectrograph were 150 grooves/mm blazed at 500 nm and 1800 grooves/mm blazed at 300 nm for determining temperature and electron density, respectively. Two 10 cm lenses were used to collimate and focus the plasma light emission onto 100 μm entrance slit for temperature measurements, while a 30 μm entrance slit was used for the density calculations for minimizing instrumental broadening. A timing generator allowed for temporal analysis of the plasma properties by varying the ICCD detector delay times with respect to the laser pulse. Spatial and laser energy dependence studies on temperature and density were performed in a time integrated manner, while for temporal analysis, a gate width of 10% of the delay time was used. The ICCD used for spectral measurement was also used for recording 2-dimensional plume self-emission by positioning it perpendicular to the plasma expansion direction. An objective lens (Nikon Macrolens, f = 70-200 mm) was used to image the plume region onto the camera to record the visible radiation integrated in the wavelength range of 350–900 nm.

III. ESTIMATION OF TEMPERATURE AND ELECTRON DENSITY

Optical emission spectroscopy (OES) is a reasonably accurate and non-intrusive method for measuring various

plasma parameters. OES provides useful information, including the temperature and density of the plume along with plume species and its ionization and kinetics. Temperature calculations are accomplished by using Boltzmann method assuming the plasma is in LTE. According to the Boltzmann distribution, the population of the excited state can be written as[28]

$$n_{nm} = n_n \frac{g_m}{Z} e^{-\frac{E_m}{kT}}, \tag{1}$$

where n_{nm} is the population of the mth excited level; g_m, the statistical weight of the upper level of the transition; E_m, the excitation energy; k, Boltzmann's constant; and T, the temperature. The emission intensity, I_{nm}, of a line is related to the population of the excited level through the following relation:[28]

$$I_{nm} \approx A_{nm} n_{nm} \frac{hc}{\lambda_{nm}} = A_{nm} n_n \frac{g_m hc}{Z\lambda_{nm}} e^{-\frac{E_m}{kT}}, \tag{2}$$

where A_{nm} is the atomic transition probability and λ_{nm} is the wavelength of the line. In the simplest form, the intensity ratio of two lines can be used for inferring the excitation temperature of the plasma. However, a Boltzmann plot employing several emission lines provides more accurate estimate of the excitation temperature. For a LTE plasma, a plot of $\ln(\lambda/Ag)$ against E for several spectral lines should be a straight line and the slope of this plot corresponds to $-1/kT$. A linear fit to experimental data not only validates the assumption of a Maxwellian electron distribution but serves as a check for errors in line assignment or transition probability value. The LPP temperature is measured employing Boltzmann method using Cu I lines at 427.51, 465.11, 510.55, 515.32, 521.82 nm. A typical time integrated spectrum at 1 mm from the target with lines selected for temperature estimate and representative Boltzmann plot are shown in Figure 3.

To measure the electron density of the plasma, we used the Stark broadening method. Stark broadening of spectral lines in plasmas is caused by collisions of charged species. From these collisions, there is both a broadening of the line and a shift in the peak wavelength. There is a direct correlation between the electron density and the FWHM in angstrom (Å) of a Stark broadened line emission as shown in the following expression:[28]

$$\Delta\lambda_{\frac{1}{2}} = \left[2W\left(\frac{n_e}{10^{16}}\right) + 3.5A\left(\frac{n_e}{10^{16}}\right)^{\frac{1}{4}} * \left(1 - \frac{3}{4}N_D^{-\frac{1}{3}}\right) W\left(\frac{n_e}{10^{16}}\right)\right] \text{Å}, \tag{3}$$

where N_D is the number of particles in the Debye sphere, A is the ion bombarding parameter, W is the electron impact parameter.[28] The first term on the right side of Eq. (3) is the electron contribution to the broadening and the second term is the ion correction factor. For nonhydrogenic ions, Stark broadening is dominated by electron impact and thus the ion correction factor is negligible.[29] As a consequence the Stark broadening equation becomes

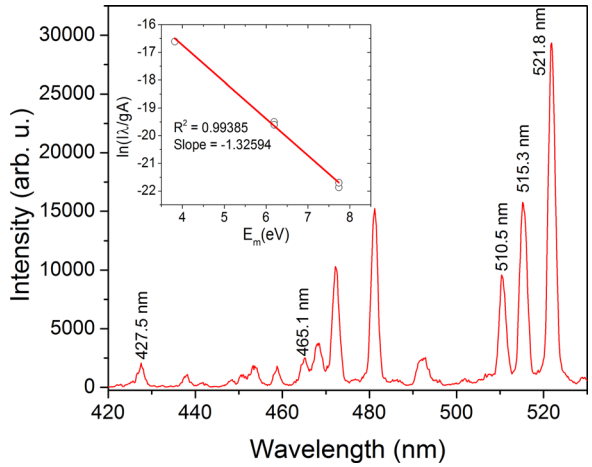

FIG. 3. Spectrum obtained at 1 mm from the brass target using Cu I lines from a 5.5 mJ fs pulse, displayed above. (Inset) A Boltzmann plot of the Cu I lines used to estimated T_{exc} (excitation temperature). The upper level energies of the emission lines are plotted against $\ln(I\lambda/Ag)$ where the slope of the line provides the temperature.

$$\Delta\lambda_{\frac{1}{2}} = 2W\left(\frac{n_e}{10^{16}}\right) \text{Å}. \tag{4}$$

Along with Stark broadening, three more broadening mechanisms may contribute to line broadening in laser ablation plasmas which include Doppler broadening, pressure broadening, and instrumental broadening. Doppler broadening is due to different Doppler shifts in different regions of the plume having different high velocity components. The estimated Doppler width for Zn I line is ~0.001 nm[30] which is negligible compared to typical Stark broadened line width and hence is ignored. The pressure broadening is proportional to the ground state number density and transition oscillator strength which is also very small and neglected.[31] Instrumental broadening has been minimized by keeping the minimum slit width of spectrograph at 30 μm. The calculated instrumental broadening with 30 μm slit was 0.025 nm. The electron density is determined using a Stark broadened line profile of Zn I spectral line centered at 481 nm ($4s5s^3S_1$-$4s4p^3P_2$). Stark broadened line profiles can be fitted with a Lorentzian profile and in our studies, the line profiles fit well with the Lorentzian profile as shown in Figure 4.

For temperature calculations, the plasma was assumed to be in LTE. In a transient system, like laser produced plasma, LTE is allowed if the collision time between particles is low compared to the time duration that significant change occurs in the plasma.[32] When the major processes of excitation and de-excitation in plasma are caused by the collision of electrons, the system is considered to be at LTE. Therefore, sufficiently large particle densities and moderately high temperatures will be required for LTE. Under the assumption of LTE, the different temperatures of the plasma, *viz.* excitation temperature (T_{exc}), the ion temperature (T_i), and the electron temperature (T_e) can be considered as $T_e \sim T_i \sim T_{exc}$. A partial requirement for LTE is to prove the validity of McWhirter criterion using[33]

$$n_e \geq 1.4 \times 10^{14} T_e^{\frac{1}{2}} (\Delta E_{mn})^3 \text{ cm}^{-3}. \tag{5}$$

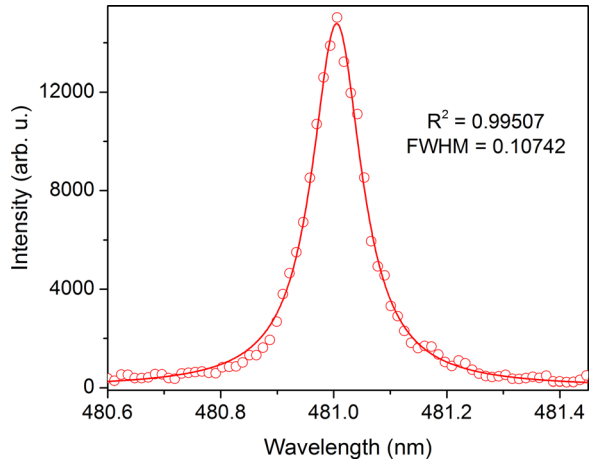

FIG. 4. The Stark broadened profile of the Zn I line used for measuring the electron density. Parameters of the Lorentz fitted profile are provided.

ΔE_{mn} is the energy difference between upper and lower energy levels in eV, T_e is the electron temperature in eV. Using the 427.5 nm line, $\Delta E_{mn} = 2.9$ eV, and thus the lowest limit for n_e is 4.8×10^{15} cm^{-3}. Our calculated values of n_e are larger than this limit, therefore the LTE approximation is assumed to be valid.

IV. RESULTS AND DISCUSSION

Understanding plasma parameters and its evolution in space and time is important for optimizing them for various applications. We analyzed visible emission from the plasma for obtaining the temperature and electron density and each was studied as a function of time, space, and laser energy for both ns and fs laser-produced plasmas. For a direct comparison between ns and fs LPP, similar laser fluence levels were maintained for spatio-temporal analysis of the plasmas though the laser irradiance differed by several orders because of ns and fs time durations of the laser pulse.

The physics of laser-plasma generation is different for fs and ns LPP due to different time scales involved in laser absorption and subsequent plasma generation. In the fs LPP case, the laser pulse interacts with the target material by depositing all of its energy into the target electrons. Since the pulse duration is too short, in fs laser ablation the τ_{ei} and t_{heat} takes place at later times $t_p \ll \tau_{ei} \sim t_{heat}$. Hence in fs LPP, ablation typically starts in the 1–10 ps time frame and is shortly followed by optical emission created from the plasma. Since the laser intensity used in the present study for fs LPP $\geq 10^{15}$ W/cm^2, at the earliest times of plasma formation the target atoms should be highly ionized and radiate in the x-ray[34] and EUV spectral window. Emission in the visible range is seen to start at longer time frames (0.1–10 ns). In the ns LPP case, the laser interacts with the target initially and immediately forms a low density plasma plume which is subsequently heated by the incoming laser pulse and can contain ionized species. Hence, the ablation and emission from the plasma happens during the duration of the laser pulse. In both ns and fs LPP, the self-emission can last up to a few hundreds of nanoseconds. This self emission is used in OES and occurs and decays in relatively the same time window for both LPPs. Typical spectrally and time integrated 2-dimensional images of the ns and fs LPP plumes recorded using ICCD are shown in Figure 5 and it clearly demonstrates the differences in hydrodynamics of ns and fs plumes. Figure 5 shows, under similar laser fluence excitation conditions, the spatial extension of the fs LPP in the plume expansion direction (along the target normal) is found to be higher compared to ns LPP.

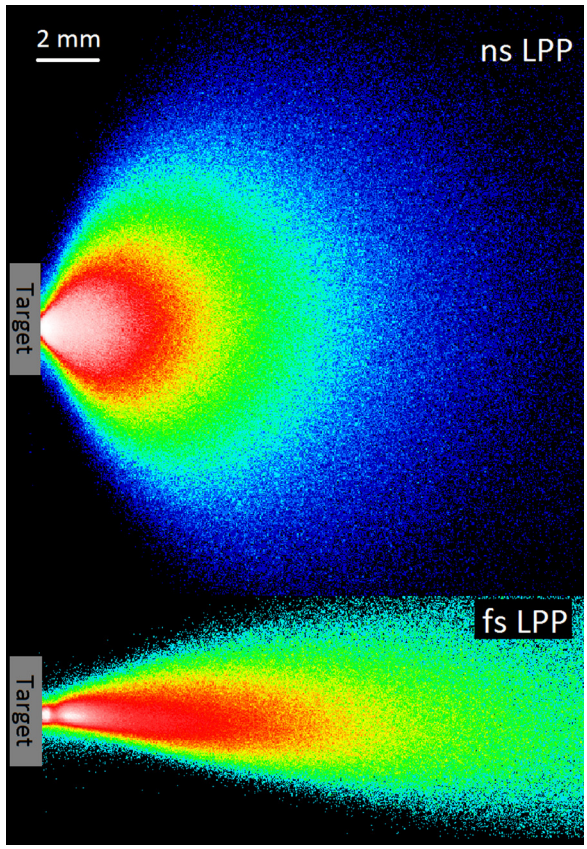

FIG. 5. Time and spectrally integrated ICCD images of ns and fs LPPs recorded under similar laser fluence conditions. The delay and integration times used for obtaining these images are 0 ns and 2 μs.

A. Time evolution of temperature and density

Typical spectra recorded from the ns and fs LPP at increasing delay times after plasma generation is given in Figure 6(a). For obtaining these spectra, a 2 μs gate was incrementally delayed to avoid early time emission from the plasma and the spectra were recorded 1 mm from the target surface with a laser energy of 5.5 mJ. Figure 6(a) clearly gives contrasting emission features of plasmas generated by ns and fs laser at similar laser fluences. Figure 6(b) shows the recorded spectra at different moments after the onset of plasma formation using a gate width of 10% of gate delay recorded at a distance 1 mm from the target. Measuring the temperature and density at early times using ns LPP can be inaccurate due to the large amount of continuum associated with the plasma, this distorts the line to continuum ratio which can create large errors associated with the relative ratios. Moreover, the excited Cu I lines were not seen during the earliest times of ns LPP evolution but appear at times $\geq$50 ns (see Figure 6(b)). Therefore, measurements of the

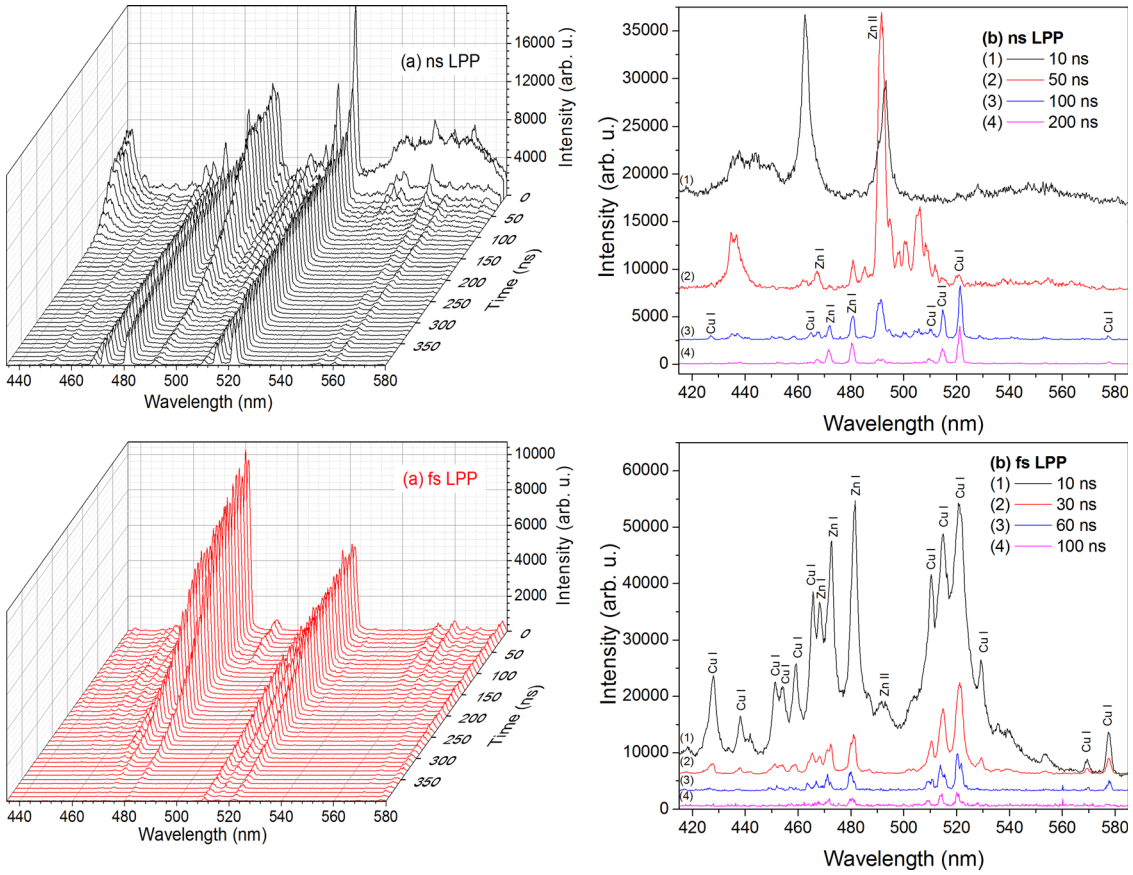

FIG. 6. (a) Typical spectra recorded from the ns and fs LPP with increasing delay times after the onset of plasma formation. A 2 μs gate width was incrementally delayed to avoid early time emission from the plasma. (b) Time resolved spectrum with gate width of 10% of the delay time obtained from ns and fs LPP. The spectra are scaled upwards for clarity and in the fs LPP, the spectra obtained at 60 ns is multiplied by a factor of five and spectra obtained at 100 ns is multiplied by a factor of ten to accent the lines. The lines identified are also marked in the spectra. All spectra were recorded at 1 mm from the target surface.

temperature could not be performed for the ns LPP until times >50 ns delay.[27] However, the fs LPP has very little continuum throughout the course of its lifetime which allows for measurements at early times of plasma evolution seen in Figure 6(b). Moreover, the fs plume mainly contained excited atoms even at the earliest time index, whereas the ns LPP contains larger number of ionic species. With the short pulses of the fs LPP, the continuum emission associated with the plasma is much weaker and lasts shorter time frames when compared to conventional ns LPP due to the association of free-free, free-bound transitions states that are caused by electron-ion recombination in the plasma alone.[35,36]

The temporal evolution of the temperature and density is of prime importance, since many kinetic reaction rates depend directly or indirectly on these parameters. The time evolution of excitation temperature recorded at 1 mm from the target surface is given in Figure 7 for both ns and fs LPP. For these studies the gate width of the ICCD intensifier is set at 10% of the delay time analyzed. The laser energy used in the experiment was 5.5 mJ.

For ns LPP, an initial excitation temperature of 10 000 K is observed at 1 mm and drops rapidly with time. A previous report showed similar trends for ns LPP, with a rapid drop in temperature after laser plasma generation with respect to time.[37,38] The time evolution of fs LPP shows a much different trend, the plasma decays slowly within the first 40 ns and then rapidly begins to drop, this profile was also reported by Xu *et al.*[39] showing a slow decay and then a drop at similar times even though there was no explanation given for the unusual decay. Our previous studies[40] as well as ICCD imaging of fs plumes (see Figure 5) showed that plasma expansion is more collimated in the fs LPP compared to ns LPP. This is also supported by the fact that under similar laser fluence conditions, the spatial extension of the plasma plume in the

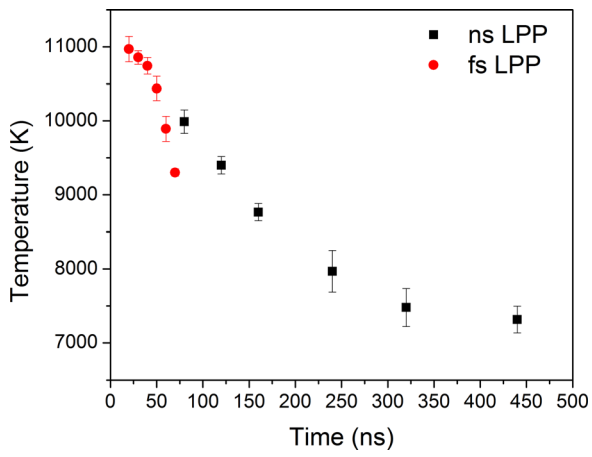

FIG. 7. Temporal evolution of the excitation temperature for ns LPP and fs LPP, using a gate width which is 10% of the chosen time delay.

present study is found to be higher for fs LPP compared to ns LPP. Hence, the plasma expansion could be more cylindrical in fs LPP.[41]

In ns LPP, the plasma expands isothermally during the laser pulse, while in fs LPP, the plasma formation happens ~1-10 ps which is a relatively long time after the termination of the laser beam (40 fs). Typically for ns LPP, plasma expansion is hemi-spherical at the leading edge and conical along its longitudinal axis during the adiabatic expansion phase which starts after the end of the laser pulse.[42] During adiabatic expansion, the thermal energy of the plasma is converted into kinetic energy causing rapid cool down of the plasma. The lifetime of the plasma emission is found to differ significantly for ns and fs LPP. Under similar fluence conditions, the line emission for the ns LPP exists at times up to hundreds of ns, while in the fs LPP scenario, very weak emission intensity is noticed after 100 ns. It should be mentioned that the observable line emission intensity depends on the gating time of the detector. In the present experiment, we used a gating time of 10% of the time analyzed for avoiding temporal mixing. The temperature measurements shown indicate that the peak value measured for fs LPP is higher than ns LPP though the peak value delay times for each LPP are different. Other studies[35] indicated the ns LPP has a temperature ~2 times larger than the fs LPP but this was measured at time indexes greater than 10 ns from the laser target interaction. The temperature of ns LPP at earliest times is not measureable in the present experiments due to the large amount of continuum. However, the fs LPP should exhibit higher temperatures in comparison the ns LPP at the earliest times due to significantly higher laser power densities used, leading to generation of a highly ionized plasma.[43] In ns LPP, the leading edge of the laser initiates the plasma and then continues to heat the plasma at high densities during expansion which improves the lifetime of plasma by imparting the majority of its energy into the ablated material in the plume rather than the target material.

Figure 8 shows the temporal evolution of the electron density for both ns and fs LPP recorded at 1 mm from the target surface at laser energy of 5.5 mJ. The temporal evolution of electron density for ns and fs LPP showed a very rapid drop due to expansion of the plume. The peak density measured for ns and fs LPPs is $1.31 \pm 0.16 \times 10^{18}\,\mathrm{cm}^{-3}$ and $5.5 \pm 0.7 \times 10^{18}\,\mathrm{cm}^{-3}$, respectively. For ns LPP, the electron density drops to half within 100 ns after the peak of the laser pulse. Comparing this to the fs LPP, the peak density was on the order of ~4.5 times greater than the ns LPP but drops much more rapidly down to a third of its original value within 30 ns. Both fs and ns LPP attain similar electron density values approximately 100 ns after the onset of plasma formation. The observation of significantly higher electron density (factor ~4.5) for fs LPP compared to ns LPP can be related to a larger amount of matter ablated from the target in the case of fs LPP. Our recent studies showed that the fs LPP produced higher kinetic energy and more mass per pulse than ns plumes over all angles with respect to target normal under similar laser fluence conditions.[40] The ion flux and kinetic energy studies show fs laser plasmas produce narrower angular distribution of charged species, while ns laser plasmas provide narrower energy distribution.[40] The decrease in electron density with time for both ns and fs LPP is due to the plasma expansion and three-body recombination of electrons with their parent ions.[30,44,45] Unnikrishnan *et al.* conducted studies on the electron density of copper from a ns LPP and has found that the temporal profile follows an exponential decay.[38] Also, Xu *et al.* conducted temporal studies using fs LPP on a Pb target and also observed exponential electron density decay for fs LPP.[39] The electron density evolution shown in Figure 8 follows the same trend of exponential decay for both ns and fs LPP as seen by other authors. However, the fs LPP density decay is found to be much more rapid than ns LPP density decay.

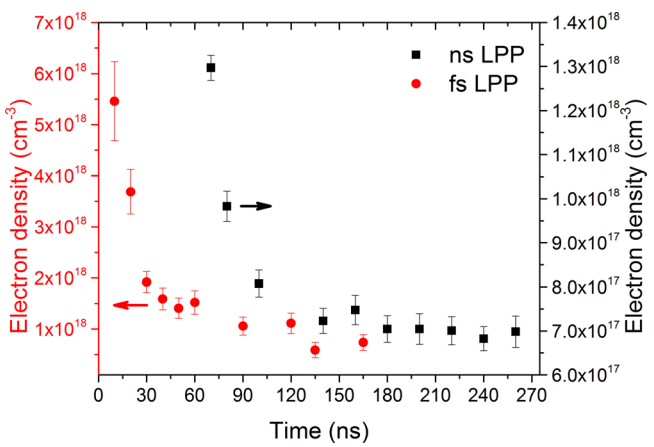

FIG. 8. Temporal evolution of electron density for ns LPP (black squares) and fs LPP (red circles) recorded at 1 mm from the target at a laser energy of 5.5 mJ. The gate width was set to 10% of the delay time and was conducted under similar conditions for both plasma plumes at a distance from the target of 1 mm.

B. Spatial dependence of temperature and density

Plasma formation occurs in a small volume containing a very high pressure heated gas which will propagate outward. This propagation depends on ambient conditions;[46,47] but under vacuum conditions, the plume expansion is increased due to very little background confinement. All LPPs have preferential expansion of the material in the direction perpendicular to the target surface, irrespective of the angle of incidence of laser beam.[37]

Figure 9 shows the temperature and electron density as a function of distance from the target. These measurements were performed in a time-integrated manner. The laser energy used in the experiment was 5.5 mJ for both lasers. Comparing ns to fs LPPs shows that the preferential expansion of the fs plume is more focused towards the target normal than the ns plume allowing for more material to be spread in a forward bias outward from the target.[40,41] Because of this, under similar fluence conditions, the spatial extension of the fs LPP in the plume expansion direction (along the target normal) is found to be higher compared to ns LPP, as seen in Figure 5. Hence the emission analysis is possible for larger distances for fs LPP (6 mm) compared to ns LPP (3 mm). The time-integrated temperature drop is more or less similar for both ns and fs LPP even though

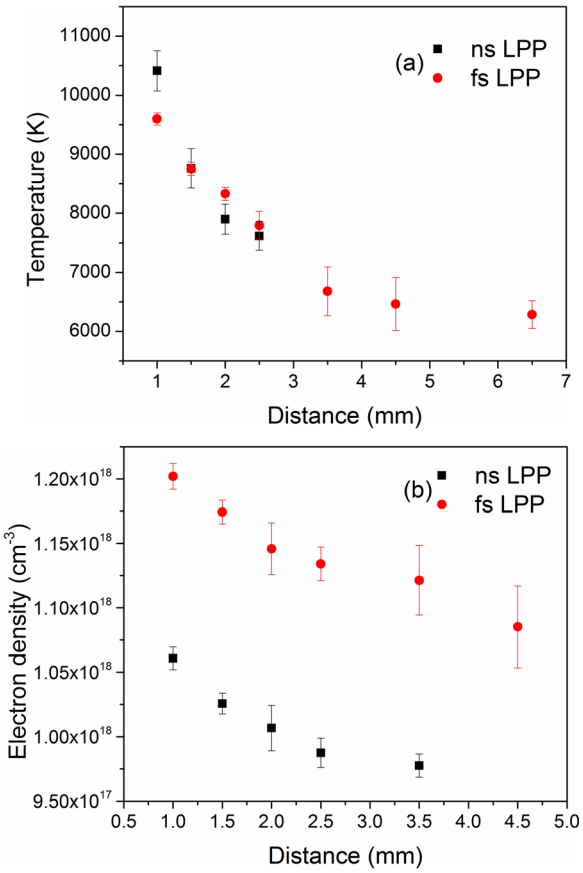

FIG. 9. Spatial analysis of (a) excitation temperature and (b) electron density for ns LPP (black squares) and fs LPP (red circles); conducted under similar laser fluence conditions. The spectral measurements were done in a time integrated manner.

higher temperatures are observed for ns LPP at shorter distances. For the ns LPP, the temperature decreases from 10 400 K to 7700 K from a distance of 1 mm to 2.5 mm, while the fs temperature decreases from 9600 K to 6400 K over a distance of 5 mm.

Figure 9(b) shows the spatial evolution of electron density for ns and fs LPPs. In both cases, the density drops with increasing distance from the target surface. Comparing ns and fs LPP, the measured density is found to be higher for fs LPP for all distances studied. With increasing distance, the density for ns LPP falls from $1.06 \pm 0.12 \times 10^{18}\,\mathrm{cm}^{-3}$ at 1 mm to $9.77 \pm 0.14 \times 10^{18}\,\mathrm{cm}^{-3}$ at 3.5 mm, while for fs LPP, n_e drops from $1.20 \pm 0.10 \times 10^{18}\,\mathrm{cm}^{-3}$ at 1 mm to $1.08 \pm 0.23 \times 10^{18}\,\mathrm{cm}^{-3}$ at 4.5 mm. Higher electron density in the fs LPP is expected as the fs laser ablates more material compared to the ns LPP[21,48] due to efficient laser-target coupling. Though fs LPP showed higher density irrespective of the spatial position studied, the measured density drops are minimal. However, for both ns and fs LPPs, the density values changed significantly with respect to time as shown in Figure 8. It should be noted that temperature and density values given in Figure 9 estimated at various distances are indicative of the average local conditions (time-averaged) rather than the defining conditions at a particular stage of the plasma's evolution. It also indicates plasma is highly transient and hence its parameters change very rapidly in time especially in the first 100 ns. Similarly, large variation in density and temperature can be expected at very short distances (<1 mm) both in the axial (along the plume expansion direction) as well as in the radial directions.[49] Previous reports showed the density reduction with distance followed approximately 1/z law indicating the initial expansion of the plume is one-dimensional.[50] These electron densities follow similar profiles previously reported for ns LPP, but this study had lower temperatures due to a lower laser power density used than the previous studies.[50–52]

C. Laser energy dependence of temperature and density

LPP characteristics depend greatly on the laser energy. The changes in laser energy can influence both laser-target absorption mechanisms as well as laser ablation mechanisms though the physics of both processes differ for ns and fs LPP. The incoming energy can affect the temperature, density, ablated mass, and ion energies.[40] Figure 10 shows the temperature and electron density of the brass plasma with respect to laser energy at a distance of 1 mm from the target surface. These measurements were done in a time-integrated manner. The laser energy was varied between 1 and 6 mJ by keeping similar laser focus spot for ns and fs laser excitation. The emission intensity was found to be very weak for 1 mJ ns laser ablation and hence the density and temperature measurements were not preformed. Previous studies showed

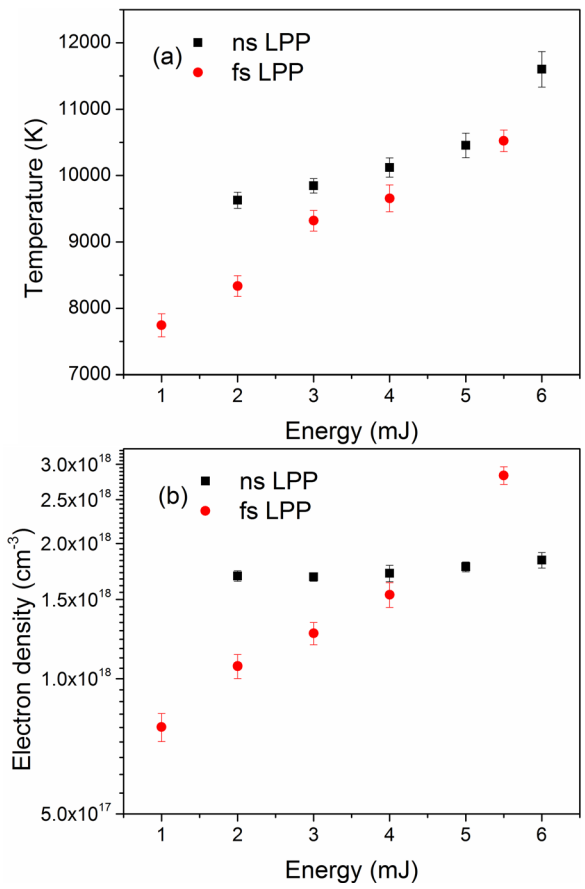

FIG. 10. Time integrated energy analysis of (a) excitation temperature and (b) electron density for ns LPP (black squares) and fs LPP (red circles); conducted at different energies, 1 mm from the target, and similar spot size.

that the laser ablation threshold fluence is lower for ultrashort pulse laser ablation compared to ns long pulse ablation.[23] The estimated ablation threshold fluence for Cu is 0.4 J/cm^2 and 3 J/cm^2 for 100 fs and 6 ns laser pulse durations.[23] The differences in ablation thresholds for ultrashort and long pulses are due to differences in laser absorption mechanisms as well as in changes in electron to lattice energy exchange time. For ultrashort pulses, $\tau_{ei} \sim t_{heat} \gg t_p$, while for ns long pulses $t_p \gg (\tau_{ei}; t_{heat})$. The temperature measured, Figure 10(a), shows a linear increase as the laser energy increases for both ns and fs LPPs. Previous studies have shown a linear increase in the temperature and electron density for ns LPP but the energy ranges used were much greater than this study.[27] The linear slope of the ns LPP is smaller than the fs slope by ~40% indicating that the fs LPP is more dependent on laser energy than ns in this energy range.

Figure 10(b) shows the laser energy dependence on the electron density for ns and fs LPP. The ns LPP's slope is 3.5×10^{16} (cm^3 mJ)$^{-1}$ which is one order of magnitude lower than that of the fs LPP at 3.6×10^{17} (cm^3 mJ)$^{-1}$. Therefore, there is a very strong laser energy dependence on electron density associated with the fs plasma. The variation in density is more pronounced and can be understood considering the laser-plasma interaction in ns LPP. In ns LPP, after plasma generation, the rest of the energy is used for reheating and hence minimal change is density is expected. In the fs LPP scenario, the entire energy is coupled to target and more particles are generated.[40] Hence we can expect larger energy dependence for fs LPP as compared to ns LPP.

V. CONCLUSIONS

We investigated the temporal and spatial evolution of excitation temperature and electron density of fs and ns laser-produced metal plasmas. The excitation temperature measurement was performed using the Boltzman plot method using multiple Cu I lines, while electron density was measured using the Stark broadened profile of Zn I line. For systematic comparison, similar laser fluence levels were maintained for both ns and fs plasmas, though the laser power densities at the target surface differed by 5 orders of magnitude.

The continuum for fs LPP is greatly reduced compared to the ns LPP allowing for detailed analysis at the earliest time of plume evolution, while large continuum is noticed for ns LPP at times <50 ns. The time-resolved spectral analysis also showed that the fs LPP spectra are dominated by excited neutrals at the initial times, while the ns LPP spectra are dominated by ions along with continuum. The ns LPP temporal analysis of temperature showed a sharp drop from $10\,100 \pm 1150$ K at the earliest measurement times, while the fs temperature decreased at a slower rate from $10\,900 \pm 1300$ K at initial times although the time scales measured for both were measurably different. The drop in temperature for ns and fs LPP is due to adiabatic expansion and three body recombination. The density analysis showed rapid exponential decay with time also associated with adiabatic expansion, however, the fs LPP showed higher density values at initial times and both ns and fs LPPs obtain similar densities at times >100 ns. The peak densities estimated for fs and ns LPPs are $5.5 \pm 0.65 \times 10^{18}$ cm^{-3} and $1.3 \pm 0.08 \times 10^{18}$ cm^{-3}, respectively. The higher density observed at earlier times for fs LPP is attributed to the larger amount of material ablated from the target where plasma shielding is absent.

Observing the spatial distribution of both ns and fs LPPs, the temperature profiles had similar decays but the fs LPP plume parameters were measurable at distances much further up to 7 mm from the target, while the ns LPP which were only measurable up to 3 mm. This may be due to collimated expansion of the fs plasma from the target. Under similar fluence conditions, the time integrated spatial analysis of density showed consistently higher values for fs LPP which is associated with the larger amount of material ablated from the target. The laser energy dependence on temperature and electron density exhibited linear increases in both cases, though rapid rise in both temperature and density were evident in fs LPP. The slope of the fs LPP excitation temperature with laser energy was 40% larger than that of the ns LPP. The difference in the excitation temperature slope with respect to laser energy is attributed to differences in laser-target and laser-plasma coupling for ns and fs LPP. For fs LPP, the entire energy is deposited in the target, while in the ns LPP, a large part of energy is deposited in the plasma plume after its generation.

ACKNOWLEDGMENTS

This work was partially supported by the U.S. DOE, Office of National Nuclear Security Administration (NNSA) under Award Nos. DE-NA0000463 and DE-NA0001174.

[1]X. Zeng, X. L. Mao, R. Greif, and R. E. Russo, Appl. Phys. A **80**, 237 (2005).
[2]N. H. Rizvi, RIKEN Rev. **50**, 107 (2003).
[3]G. Cerullo, R. Osellame, S. Taccheo, M. Marangoni, D. Polli, R. Ramponi, P. Laporta, and S. De Silvestri, Opt. Lett. **27**, 1938 (2002).
[4]V. Kara and H. Kizil, Opt. Lasers Eng. **50**, 140 (2012).
[5]R. M. Kurtz, J. A. Squier, V. M. Elner, D. Du, X. B. Liu, A. Sugar, and G. A. Mourou, Invest. Ophthalmol. Visual Sci. **35**, 1786 (1994).
[6]B. X. Hou, J. Nees, J. Easter, J. Davis, G. Petrov, A. Thomas, and K. Krushelnick, Appl. Phys. Lett. **95**, 101503 (2009).
[7]H. E. Bennett, SPIE **2376**, 21 (1995).
[8]T. Donnelly, J. G. Lunney, S. Amoruso, R. Bruzzese, X. Wang, and X. Ni, J. Appl. Phys. **108**, 043309 (2010).
[9]T. Donnelly, J. G. Lunney, S. Amoruso, R. Bruzzese, X. Wang, and X. Ni, Appl. Phys. A **100**, 569 (2010).
[10]D. Yadav, V. Gupta, and R. K. Thareja, J. Appl. Phys. **106**, 064903 (2009).
[11]J. Badziak, A. A. Kozlov, J. Makowski, P. Parys, L. Ryc, J. Wolowski, E. Woryna, and A. B. Vankov, Laser Part. Beams **17**, 323 (1999).
[12]K. P. Jochum, B. Stoll, K. Herwig, A. Amini, W. Abouchami, and A. W. Hofmann, Int. J. Mass Spectrom. **242**, 281 (2005).
[13]G. S. Senesi, M. Dell'Aglio, R. Gaudiuso, A. De Giacomo, C. Zaccone, O. De Pascale, T. M. Miano, and M. Capitelli, Environ. Res. **109**, 413 (2009).
[14]B. Toftmann, M. R. Papantonakis, R. C. Y. Auyeung, W. Kim, S. M. O'Malley, D. M. Bubb, J. S. Horwitz, J. Schou, P. M. Johansen, and R. E. Haglund, Thin Solid Films **453**, 177 (2004).
[15]Y. Hirayama and M. Obara, J. Appl. Phys. **97**, 064903 (2005).
[16]C. R. Phipps, *Laser Ablation and Its Applications* (Springer, New York, 2007).
[17]E. L. Gurevich and R. Hergenroeder, Appl. Spectrosc. **61**, 233A (2007).

[18]B. Rethfeld, K. Sokolowski-Tinten, D. von der Linde, and S. I. Anisimov, Appl. Phys. A **79**, 767 (2004).
[19]H. S. Lim, and J. Yoo, J. Mech. Sci. Technol. **25**, 1811 (2011).
[20]J. Koch, A. von Bohlen, R. Hergenroder, and K. Niemax, J. Anal. At. Spectrom. **19**, 267 (2004).
[21]S. Canulescu, E. Papadopoulou, D. Anglos, T. Lippert, M. J. Montenegro, S. Georgiou, M. Dobeli, and A. Wokaun, Appl. Phys. A **105**, 167 (2011).
[22]S. Yalcin, Y. Y. Tsui, and R. Fedosejevs, J. Anal. At. Spectrom. **19**, 1295 (2004).
[23]E. G. Gamaly, A. V. Rode, B. Luther-Davies, and V. T. Tikhonchuk, Phys. Plasmas **9**, 949 (2002).
[24]W. H. Tao and H. K. Yasuda, Plasma Chem. Plasma Process. **22**, 297 (2002).
[25]H. Tojo, A. Ejiri, J. Hiratsuka, T. Yamaguchi, Y. Takase, K. Itami, and T. Hatae, Rev. Sci. Instrum. **83**, 023507 (2012).
[26]Z. Wang, G. X. Zhang, Q. Zhang, and Z. D. Jia, IEEE Trans. Plasma Sci. **40**, 1380 (2012).
[27]S. S. Harilal, C. V. Bindhu, R. C. Issac, V. P. N. Nampoori, and C. P. G. Vallabhan, J. Appl. Phys. **82**, 2140 (1997).
[28]H. R. Griem, *Plasma Spectroscopy* (McGraw-Hill, New York, 1964).
[29]H. R. Griem, *Principles of Plasma Spectroscopy* (Cambridge University Press, Cambridge, England; New York, 1997).
[30]D. N. Patel, P. K. Pandey, and R. K. Thareja, Appl. Opt. **51**, B192 (2012).
[31]Y. P. Liu, C. Gao, J. L. Zeng, and J. R. Shi, Astron. Astrophys. **536**, A51 (2011).
[32]A. A. Voevodin, S. J. P. Laube, S. D. Walck, J. S. Solomon, M. S. Donley, and J. S. Zabinski, J. Appl. Phys. **78**, 4123 (1995).
[33]G. Bekefi, *Principles of Laser Plasmas* (Wiley, New York, 1976).
[34]L. U. Labate, Ph.D. dissertation, University of Bologna, Italy, 2004.
[35]A. De Giacomo, M. Dell'Aglio, A. Santagata, and R. Teghil, Spectrochim. Acta, Part B **60**, 935 (2005).
[36]B. Le Drogoff, J. Margot, M. Chaker, M. Sabsabi, O. Barthelemy, T. W. Johnston, S. Laville, F. Vidal, and Y. von Kaenel, Spectrochim. Acta, Part B **56**, 987 (2001).
[37]T. Wu, X. B. Wang, S. Y. Wang, J. Tang, P. X. Lu, and H. Lu, J. Appl. Phys. **111**, 063304 (2012).
[38]V. K. Unnikrishnan, K. Alti, V. B. Kartha, C. Santhosh, G. P. Gupta, and B. M. Suri, Pramana, J. Phys. **74**, 983 (2010).
[39]H. L. Xu, J. Bernhardt, P. Mathieu, G. Roy, and S. L. Chin, J. Appl. Phys. **101**, 033124 (2007).
[40]B. Verhoff, S. S. Harilal, and A. Hassanein, J. Appl. Phys. **111**, 123304 (2012).
[41]R. Teghil, L. D'Alessio, A. Santagata, M. Zaccagnino, D. Ferro, and D. J. Sordelet, Appl. Surf. Sci. **210**, 307 (2003).
[42]R. K. Singh and J. Narayan, Phys. Rev. B **41**, 8843 (1990).
[43]S. N. Srivastava, K. Rohr, and B. K. Sinha, J. Appl. Phys. **99**, 073301 (2006).
[44]M. Capitelli, A. Casavola, G. Colonna, and A. De Giacomo, Spectrochim. Acta, Part B **59**, 271 (2004).
[45]P. K. Pandey and R. K. Tharejaa, Phys. Plasmas **18**, 033505 (2011).
[46]K. F. Al-Shboul, S. S. Harilal, and A. Hassanein, Appl. Phys. Lett. **99**, 131506 (2011).
[47]K. F. Al-Shboul, S. S. Harilal, and A. Hassanein, Appl. Phys. Lett. **100**, 221106 (2012).
[48]A. H. Dogar, B. Ilyas, H. Qayyum, S. Ullah, and A. Qayyum, Eur. Phys. J.: Appl. Phys. **54**, 10301 (2011).
[49]M. Polek, S. S. Harilal, and A. Hassanein, Appl. Opt. **51**, 498 (2012).
[50]S. S. Harilal, B. O'Shay, M. S. Tillack, and M. V. Mathew, J. Appl. Phys. **98**, 013306 (2005).
[51]S. Canulescu, E. L. Papadopoulou, D. Anglos, T. Lippert, C. W. Schneider, and A. Wokaun, J. Appl. Phys. **105**, 063107 (2009).
[52]P. Yeates and E. T. Kennedy, J. Appl. Phys. **108**, 093306 (2010).